

# Intrinsic local symmetry-breaking in nominally cubic paraelectric BaTiO<sub>3</sub>

Xin-Gang Zhao,<sup>1</sup> Oleksandr I. Malyi,<sup>1</sup> Simon J.L. Billinge,<sup>2</sup> and Alex Zunger<sup>1,\*</sup>

1. Renewable and Sustainable Energy Institute, University of Colorado, Boulder, Colorado 80309

2. Department of Applied Physics and Applied Mathematics, Fu Foundation School of Engineering and Applied Sciences, Columbia University, New York, NY 10027

\*Corresponding author email: [Alex.Zunger@colorado.edu](mailto:Alex.Zunger@colorado.edu)

Whereas low-temperature ferroelectrics have a well understood ordered spatial dipole arrangement, the fate of these dipoles in paraelectric phases remains poorly understood. This is studied here as an energy minimization problem using both static and molecular dynamic (MD) density functional theory (DFT). We find that considering the non-thermal internal energy already reveals the formation of a distribution of static local displacements that (i) mimic the symmetries of the low temperature phases, while (ii) being the precursors of what high temperature DFT MD finds as thermal motifs.

Oxide perovskites  $ABO_3$ , typified by  $BaTiO_3$  (BTO), have local dipoles  $\{\mu^{(i)}_{local}\}$ , formed by polar atomic displacements off high symmetry positions  $i$ . At low temperatures, these can organize into ferroelectric (FE) long-range-ordered (LRO) structures. In contrast, above the Curie temperature  $T_c \sim 401$  K, BTO transforms into a cubic paraelectric (PE) phase.[1] Crystallographically, this high-temperature BTO structure—as well as the experimentally reported  $\sim 90$  other oxides  $ABO_3$ [2,3] and scores of halide[4,5] perovskites are classified as cubic Pm-3m space group symmetry. A central question in this field[6–14] regards the nature of the spatial configurations of the local  $\{\mu^{(i)}_{local}\}$  dipoles in the paraelectric phase. Suppose the Pm-3m cubic paraelectric phase, consisting of a single, undeformed octahedral motif as its repeat unit (the monomorphous configuration), is taken literally, rather than as a ‘virtual crystal’ average over configurations. In this case, the PE phase will not only have vanishing global dipole moment  $\mu_{global} \sim 0$ , but also vanishing local dipoles on each site,  $\{\mu^{(i)}_{local} = 0\}$  (a ‘non-electric’ configuration; Fig. 1a). Experimentally, in contrast, the pioneering 1968 diffuse scattering XRD measurements of Comes et al.[9] on the PE phase were interpreted as being due to the presence of nonzero local dipoles  $\{\mu^{(i)}_{local}\}$  that persist locally in the high-temperature cubic phase of BTO. Other measurements also seem to indicate the off-centering of the Ti ions not only in the low temperature FE phases, but also in the PE phase. This includes Nuclear Magnetic Resonance (NMR),[10] atomic pair distribution function (PDF) analysis of neutron powder diffraction data,[11–13] X-ray absorption fine structure (EXAFS),[14] as well as the observation of birefringence,[15] second harmonic generation (SHG),[16] and piezoelectricity in cubic oxide paraelectrics.[17,18] These effects, however, are forbidden in the centrosymmetric nominal cubic phase, suggesting that locally the symmetry is lower. Although some sightings of such ‘forbidden symmetries’ appear to involve *extrinsic* factors (such as defects[19] or growth-induced microstructures[20]), there are cases, most prominently BTO,[21] where intrinsic factors of symmetry-breaking appear to be at play. Other experiments, most notably inelastic neutron scattering,[22,23] suggest that the local dipoles appear only on cooling through the ferroelectric phase transition. The resulting controversy has held the perovskite community in fascination for over 50 years. This can be posed in the following way: Is the paraelectric condition of  $\mu_{global} \sim 0$  realized by having (a)  $\{\mu^{(i)}_{local} = 0\}$  (symmetry unbroken, absence of local dipoles, as illustrated in Fig. 1a) or (b) via distribution of mutually compensating nonzero local dipoles  $\{\mu^{(i)}_{local} \neq 0\}$  (Fig. 1b). What makes the resolution of this conundrum important is that the choice between (a) vs. (b) strongly affects the nature of predictions of calculations of spectroscopic and transport properties. For example, the use of the monomorphous view (a) ubiquitous in standard databases[24–27] as input to calculations often leads to a significant underestimation of band gaps.[28–31] On the other hand, possibility (b) has been generally interpreted by assigning local dipoles in the PE phase to *thermal fluctuations*, where atoms are oscillating thermally around their Wyckoff positions and time averaging to a zero polarization. However, such thermal effects do not account for the static nature of the polarization implied by the macroscopic experiments.[32] Indeed, in principle, there is also a possible contribution from modes driven by intrinsic chemical bonding effects even before thermal motion is considered. These are known in inorganic compounds, such as degeneracy removal exemplified by the Jahn-Teller distortions of  $d$  orbital impurities in insulators,[33] or by the lone-pair  $s$  orbitals of Sn, Pb, or Bi centers in inorganic compounds,[34] or via sterically-induced octahedral rotations and tilting in perovskites,[35] all understood as a-thermal energy lowering symmetry-breaking. Here, we will determine if the symmetry breaking is driven by intrinsic chemical bonding effects (obtainable by minimizing internal energy  $U_0$ ) or by the dynamic thermal effects (obtainable in molecular dynamics by  $U_0$ -TS). We find that the former

effect (hereafter referred to as *statically-induced*) is the causal driving force for symmetry breaking in paraelectric phase, even though at finite temperature both statically-induced and dynamic contributions exist.

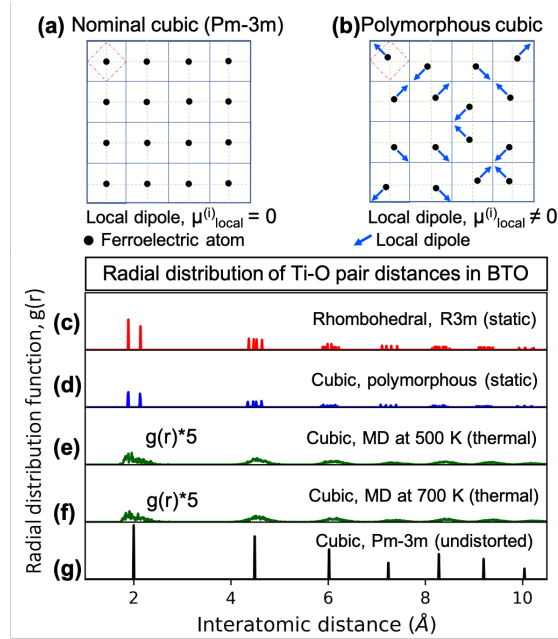


**Figure 1.** Schematic illustrations of displacements in models of paraelectric BaTiO<sub>3</sub> (a) nominal cubic, (b) polymorphous cubic and [(c)-(g)] Ti-O radial pair distribution functions (RPDF). Here, (c) is the RPDF for the static rhombohedral phase (1fu/cell, red line), (d) is for the static polymorphous network (blue line), and (e) and (f) are from snapshots of MD simulation in the NPT mode for P=1 atm, T=500 and 700 K. Finally, (g) shows RPDF in nominal cubic phase (1 fu/cell, black line). No smearing was applied to the plots.

Here, we theoretically investigate the evidence in PE phases for non-thermal static as well as dynamic thermal effects from density functional theory (DFT), using a common supercell representation allowing symmetry-breaking, should it lower the energy. We find that (i) the local symmetry-breaking in paraelectric BTO has a significant *static* origin (i.e., evident already from minimizing the internal energy  $U_0$ ). (ii) Projecting the relaxed displacements onto irreducible representation (irreps) of the parent cubic structure results in  $\Gamma_4^-$ ,  $\Delta_5$ ,  $M_2^-$ , and  $X_5^+$  as dominant modes (Fig. 2). Here,  $\Gamma_4^-$  is the ferroelectric mode inherited from the low-temperature long-range-ordered phase (Fig. 2a), whereas  $M_2^-$  is the anti-ferroelectric (AFE) mode in the ordered I-43m structure (Fig. 2b).[36] The presently predicted energy lowering modes agree with the dominant modes found by Senn et al.[11] by selecting atomic displacements that fit their measured PDF data; (iii) The local modes identified from minimization of the internal energy  $U_0$  are precursors of what we find in high temperature DFT MD simulations as *thermal effects associated with the free energy*  $U_0-TS$ . These findings are different than the conventional single parabolic free energy vs. local dipole common in paraelectrics when static distortions are ignored. This study underscores the importance of using a polymorphous approach more generally when using DFT to study phases that may have local symmetry breaking, such as PE phases. But these ideas can also apply

more broadly to other para phases made of different local motifs such as local magnetic moments[37,38] or local structural deformations in halide perovskites.[39]

*Current approach in context of previous work:* The questions regarding the microscopic nature of PE phases were historically discussed in the language of "displacive"[36] vs. "order-disorder", [6–8] that grew up to fit observations to the Landau-esque phonon-softening phase transition theory work of the 1970s. In the displacive case, at high temperatures, atoms are moving in wide potential wells, whose minima are, nonetheless, at the crystallographic Wyckoff positions. On the contrary, in the order-disorder case,[6] ions reside in static displaced potential minima and make infrequent hops to other displaced minima. The average symmetry is recovered by averaging over all atomic displacements presented in the manner of the original Comes model.[9] These pictures are intuitive and have a well-developed empirical modeling framework (Landau theory). However, computational realizations of such classic perspectives have struggled for a long time to predict the main experimental observations. Zhang et al.[36] attempted to handle the microscopic structure of the cubic PE phase by a specific choice of a long-range-ordered  $2 \times 2 \times 2$  supercell. In their work, the authors chose a periodic, LRO structure (space group  $I-43m$ ) that has a single AFE mode ( $M_2^-$  type), rather different than the multi-modes found later by Senn et al.[11] Furthermore, BTO does not have a bona fide crystallographic AFE phase.[1] Also, the zero net polarization  $\mu_{\text{global}} = 0$ , predicted[36] is in conflict with measurements above  $T_c$ , [40,41] suggesting there is more to the story.

To understand the possible significance of symmetry-breaking within the PE phase and whether it emerges from static or dynamic effects, we use a polymorphous DFT (polyDFT) approach.[38,39] In brief, it (i) does not restrict the *local* symmetry of the PE phase to that of a monomorphous primitive structure having a single local motif, (ii) does not use a long-range-ordered dipole model for the PE phase,[36] and (iii) explores both static (via minimization of the internal energy  $U_0$ ) and dynamic (via thermal evolution of the free energy  $F=U_0-TS$  in first-principles molecular dynamics, where  $S$  is entropy). To allow unimpeded local symmetry-breaking whilst respecting the *global* cubic symmetry, we constrain the lattice vectors to the macroscopically observed cubic shape but relax the internal energy  $U_0$  by allowing atoms to relax off high symmetry positions to minimize quantum forces on them. We use enlarged unit cells (here, 32 formula units (fu) containing 160 atoms; the results are stable against further cell enlargement). Supplementary Table S-1 demonstrates the rather weak dependence of the result on the initial configuration and on the random atomic nudges used to initialize the minimization. In this approach, the nature of the microscopic motifs in the para phase is determined by predictive energy minimization in a large supercell, rather than by modeling it at the outset as a single [36] or a couple of ordered structure.

*The distribution of Ti-O atomic pairs in paraelectric phase (Fig. 1):* We consider the partial radial distribution function (PRDF),  $g(r)_{ab}$ , between species  $a$  and species  $b$  defined as

$$g(r)_{ab} = \frac{1}{N_a} \sum_{i=1}^{N_a} \frac{\sum_{j=1}^{N_b} \delta(|r_{ij}-r|)}{4\pi r^2 dr} \quad (1)$$

where  $N_a$  and  $N_b$  refer to the total number of atoms for each species and  $r_{ij}$  is the length of the vector from atom  $i$  to atom  $j$ . The PRDF of Ti-O pairs in the ground ferroelectric rhombohedral structure is shown in Fig. 1c and compared with the results of the polymorphous PE cubic network with static distortion (blue lines Fig. 1d) and with snapshots at 500 and 700 K of the MD profile (Fig. 1e, f). Significantly, we find, in the polymorphous cubic PE phase, a splitting of the nearest-neighbor Ti-O peak (Fig. 1d). This splitting is due to the emergence of the set of local Ti off-center displacements (Fig. 1c). No constraint is placed on

the directions of symmetry lowering displacements in the DFT calculations, which are guided simply by lowering the internal energy. However, we note that the displacements occur predominantly along {111} directions, which is consistent with the ground-state rhombohedral structure and the experimental observations of local structural probes,[9,11,14] resulting in the formation of three short (1.88 Å) and three long (2.13 Å) Ti-O bonds. A remnant of the nearest-neighbor Ti-O bond splitting is also observed in PRDFs obtained from our finite temperature MD calculations at temperatures of 500 and 700 K (green lines shown in Fig. 1e, f). Interestingly, the polymorphous cubic PE phase also has local structural motifs that are not present in either the nominal cubic monomorphous approximant (Fig. 1g) or the low-temperature ferroelectric phase (Fig. 1c). The PRDF of the Ba-Ba, Ti-Ti, Ba-O, and O-O pairs in the polymorphous network (Fig. S-1) show relatively small broadening in the range of 1-8 Å. This might be because of the Goldschmidt tolerance factor [42] $t_{eff} = \frac{R_A+R_O}{\sqrt{2}(R_B+R_O)}$  of cubic BTO (1.06) is slightly larger than one, so octahedral tilting/rotation or A site displacements are small.

*Internal energy-driven local symmetry breaking:* The characteristic of a polymorphous[38,39] phase of a material is that the total energy per atom is seen to initially decrease as the supercell size increases before saturating at a certain supercell size. We find that **cubic** BTO is polymorphous (average energy reduction -21 meV per formula unit relative to the monomorphous approximation), with predominantly Ti off-center displacements (Fig. 1d). Not all materials are polymorphous. Indeed, we find that this is the case for BTO in its ground-state rhombohedral structure (R3m, SG: 160). There is no energy reduction on increasing the cell size.

*The decomposition of static and dynamic distortion fields in terms of irreducible representations of the cubic Pm-3m symmetries (Fig.2):* The polyDFT calculations show a local symmetry-breaking in cubic BTO although this calculation step excludes any effects due to the finite temperature. This points to an intrinsic energetic driving force for forming local distortions under the set of constraints given. It is interesting to inquire what is the ‘genetic origin’ of the intrinsic symmetry-breaking mode symmetries in the PE phase. We find that these symmetries are inherited from the low-temperature long-range ordered ferroelectric phase, albeit without the long-range dipolar order. The low-temperature ferroelectric rhombohedral phase is a condensation of just one of these modes, the one associated with the  $\Gamma_4^-$  irrep (Fig. 2a). We find that in the intrinsic static polymorphous model of the PE phase, the projected  $\Gamma_4^-$  irrep mode onto Pm-3m structure is still the most prominent one (Fig. 2b), resulting in a Ti off-centering that is almost as large (0.18 Å) as in the rhombohedral phase (0.20 Å). However, the  $\Gamma_4^-$  is not the only significant mode that is populated in the polymorphous network. Two additional modes--  $\Delta_5$  and  $X_5^+$ -- both with AFE patterns have significant amplitudes. These modes originate from relative Ti displacements along opposite {100} directions in different TiO<sub>2</sub> layers. For  $X_5^+$ , the AFE-like Ti displacements occur in adjacent TiO<sub>2</sub> layers, whereas for  $\Delta_5$ , the AFE-like Ti displacements occur in three TiO<sub>2</sub> layers, in which the Ti displacements in the middle TiO<sub>2</sub> layer are not displaced. These additional  $\Delta_5$  and  $X_5^+$  modes have distortion magnitudes in the range of 0.05-0.10 Å. Importantly, they robustly appear in all independently restarted polymorphous calculations (Table S-1), suggesting they are a robust part of the polymorphous state and not due to incomplete sampling. Since  $\Delta_5$  and  $X_5^+$  are absent in the globally rhombohedral phase, presumably, they play a role in relaxing the local distortion back towards the globally cubic unit cell.

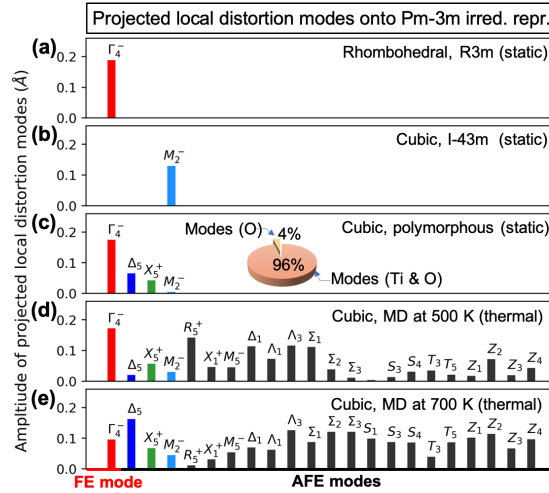


**Figure 2.** Projected distortion modes related to Ti and oxygen displacements onto parent undistorted cubic (Pm-3m) irreducible representations of (a) ground state rhombohedral structure, (b) *ordered* anti-ferroelectric cubic phase (I-43m), (c) the polymorphous structure with static distortions, and (d, e) average of 10 snapshots with interval 0.25 ps on equilibrium trajectory of Molecular Dynamic simulations with NPT ensemble at 500 and 700 K. Insert to c shows the indicated modes projected onto atomic displacements. The heights of bars in (d, e) refer to the averaged amplitude for each of the 10 snapshots.  $\Gamma_4^-$  is a ferroelectric (FE)-like Ti displacements, whereas the rest of the mode are anti-ferroelectric (AFE)-like relative Ti displacements.

**Thermal effects on paraelectric modes:** To capture thermal effects, we use MD simulations (described in Supplementary computational details) starting from the static polymorphous results. The MD runs result in atomic configurations that can also be decomposed onto the basis of the distortional modes of irreps as was done for the polyDFT relaxed structures in Fig. 2c. As expected, as the temperature is raised, many additional modes become significantly populated. For example, the mode population averaged over 10 snapshots in MD simulation at 500 and 700 K are shown in Fig. 2(d,e), indicating that the  $\Gamma_4^-$  symmetry mode remains the most prominent one at 500 K, i.e., well into the PE phase. It is still prominent at 700 K, but not necessarily dominant at that point. The  $\Gamma_4^-$  symmetry mode agrees with experimentally statements by fitting distortion modes to experimental PDF,[11] suggesting the DFT+MD approach is capturing the physics correctly.

**The net polarity in the paraelectric phase and its dependence on temperature (Fig.3):** The projections described above give important insights into the nature of the collective distortion modes of the system, but it gives incomplete information about the polarizability of the material. To quantify this, we need to consider the size of the local electric dipoles  $\{\mu_{\text{local}}^{(i)}\}$ , which are proportional to the displacements of Ti atoms away from the center of their local  $\text{O}_6$  octahedral hosts. These Ti displacements can be represented in a stereographic projection onto the XY plane of the octahedron, and then plotted for all the octahedra. This projection is shown in Fig. 3a. Figure 3b shows these projected intrinsic *static* Ti displacements of 9 independently restarted polymorphous configurations (32 formula units with Ti atoms total) onto the XY plane of one undistorted octahedron in the Pm-3m structure. Fig. 3b demonstrates that none of the Ti atoms are located at the octahedral center in the polymorphous network. This effect has been ascribed

previously to the thermal effect,[43] but it emerges here from the static calculation, suggesting the origin is electronic symmetry-breaking associated with this energy lowering.

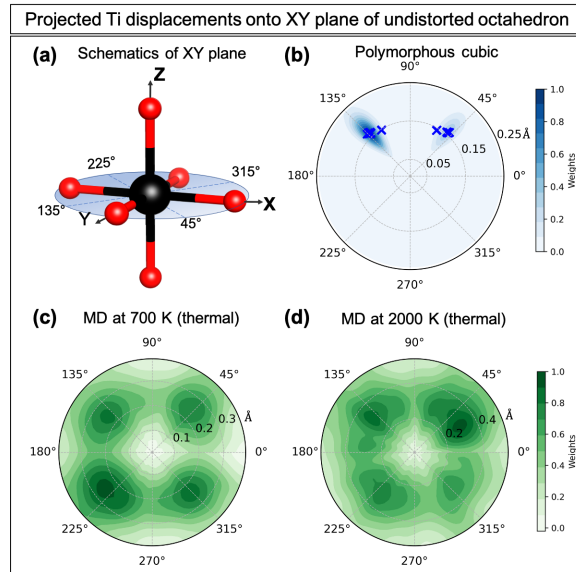


**Figure 3.** (a) Schematic XY plane of the undistorted octahedron in nominal cubic BTO. (b) The statistics of all Ti displacements (in supercell from 10 runs) projected onto XY plane in one octahedron. (c, d) The statistics of all Ti displacements in supercell projected onto XY plane in a single octahedron at 700 K within 13 ps and at 2000 K within 4 ps (see computational details of weights in Supplementary).

The ensuing static net polarization is  $\sim 0.04 \pm 0.02 \text{ \AA}$  oriented close to  $\langle 111 \rangle$  direction. Further, by averaging all dipoles over a 1 ps period on the equilibrium MD trajectories, we find that the global dipole is diminished with temperature:  $\mu_{\text{global}} = 0.021 \text{ \AA}$  at 700 K and  $\mu_{\text{global}} = 0.015 \text{ \AA}$  the temperature is 2000 K (Fig. 3c,d). This nonzero global polarization is due to the  $\Gamma_4^-$  mode (Fig. 2) with a locally FE-like pattern, whereas the weights of modes with locally AFE pattern (all modes in Fig. 2 except  $\Gamma_4^-$ ) have increased, population, thus contributing to the decrease of the global dipole. The net global polarization around the Curie temperature is not zero, in agreement with the measured polarization of single crystal BTO above  $T_c$ . [40,41] This nonzero polarization might contribute to anomalous observations, such as Raman splitting,[44] SHG,[16] piezoelectricity[17,18] and seen in PE cubic BTO. As shown in Fig. 3(c, d), the cloverleaf images show increased Ti displacements from 700 to 2000 K (close to the melting point), indicating that the picture of ‘local dipoles due to Ti atom displacements vs. free energy’ is never a single parabolic well. This finding is different from the general understanding (i.e., above the Curie temperature, the PE phase is described by the displacive model[45] as a single parabolic well, lacking static displacements.) of paraelectric phase at finite temperatures.

**In conclusion,** the blueprint of symmetry-breaking in paraelectric BTO is already determined by the minimization of the internal energy. Consequently, paraelectric BTO is polymorphous network, showing a distribution of local motifs, including locally FE-like  $\Gamma_4^-$  and AFE-like modes, but lacking long-range order. These modes persist from low- to high- temperatures with temperature dependent mode population. Likewise, Ti atoms in paraelectric BTO are always displaced from the center of the octahedron, presenting Cloverleaf-like distribution even at high temperature close to the melting point. The PE cannot be

described as the high-symmetry averaged nominal cubic structure, nor as a long-range-ordered cubic AFE phase with single type of AFE modes. Furthermore, the single parabolic potential energy surface model commonly invoked to describe PE phases (when static displacements are ignored) might not be applicable for describing the PE phase of BTO.

### Acknowledgements:

We thank fruitful discussions with Prof. Ekhard K. H. Salje and Prof. Annette Busmann-Holder on paraelectrics, and with Prof. Zhi Wang on the long-range-order model of AFE, and to Dr. Lin Ding Yuan for assistance in calculating polymorphous structures with different initial nudges shown in supplementary Table S-1. The work in the Zunger group and Billinge group was supported by the US National Science Foundation through grant DMREF-1921949. The calculations were done using the Extreme Science and Engineering Discovery Environment (XSEDE), which is supported by the National Science Foundation grant number ACI-1548562.

### References

- [1] M. B. Smith, K. Page, T. Siegrist, P. L. Redmond, E. C. Walter, R. Seshadri, L. E. Brus, and M. L. Steigerwald, *Crystal Structure and the Paraelectric-to-Ferroelectric Phase Transition of Nanoscale BaTiO<sub>3</sub>*, *J. Am. Chem. Soc.* **130**, 6955 (2008).
- [2] C. J. Bartel, C. Sutton, B. R. Goldsmith, R. Ouyang, C. B. Musgrave, L. M. Ghiringhelli, and M. Scheffler, *New Tolerance Factor to Predict the Stability of Perovskite Oxides and Halides*, *Science Advances* **5**, eaav0693 (2019).
- [3] P. V. Balachandran, A. A. Emery, J. E. Gubernatis, T. Lookman, C. Wolverton, and A. Zunger, *Predictions of New BaTiO<sub>3</sub> Perovskite Compounds by Combining Machine Learning and Density Functional Theory*, *Phys. Rev. Materials* **2**, 043802 (2018).
- [4] J. Wiktor, U. Rothlisberger, and A. Pasquarello, *Predictive Determination of Band Gaps of Inorganic Halide Perovskites*, *J. Phys. Chem. Lett.* **8**, 5507 (2017).
- [5] Q. Sun and W.-J. Yin, *Thermodynamic Stability Trend of Cubic Perovskites*, *J. Am. Chem. Soc.* **139**, 14905 (2017).
- [6] K. A. Müller and W. Berlinger, *Microscopic Probing of Order-Disorder versus Displacive Behavior in BaTiO<sub>3</sub> by Fe<sup>3+</sup> EPR*, *Phys. Rev. B* **34**, 6130 (1986).
- [7] A. Busmann-Holder, H. Beige, and G. Völkel, *Precursor Effects, Broken Local Symmetry, and Coexistence of Order-Disorder and Displacive Dynamics in Perovskite Ferroelectrics*, *Phys. Rev. B* **79**, 184111 (2009).
- [8] W. Zhong, D. Vanderbilt, and K. M. Rabe, *Phase Transitions in BaTiO<sub>3</sub> from First Principles*, *Phys. Rev. Lett.* **73**, 1861 (1994).
- [9] R. Comes, M. Lambert, and A. Guinier, *The Chain Structure of BaTiO<sub>3</sub> and KNbO<sub>3</sub>*, *Solid State Communications* **6**, 715 (1968).
- [10] R. Blinc and B. Žekš, *Dynamics of Order-Disorder-Type Ferroelectrics and Anti-Ferroelectrics*, *Advances in Physics* **21**, 693 (1972).
- [11] M. S. Senn, D. A. Keen, T. C. A. Lucas, J. A. Hriljac, and A. L. Goodwin, *Emergence of Long-Range Order in BaTiO<sub>3</sub> from Local Symmetry-Breaking Distortions*, *Phys. Rev. Lett.* **116**, 207602 (2016).
- [12] G. H. Kwei, S. J. L. Billinge, S.-W. Cheong, and J. G. Saxton, *Pair-Distribution Functions of Ferroelectric Perovskites: Direct Observation of Structural Ground States*, *Ferroelectrics* **164**, 57 (1995).
- [13] K. Page, T. Proffen, M. Niederberger, and R. Seshadri, *Probing Local Dipoles and Ligand Structure in BaTiO<sub>3</sub> Nanoparticles*, *Chem. Mater.* **22**, 4386 (2010).
- [14] B. Ravel, E. A. Stern, R. I. Vedrinskii, and V. Kraizman, *Local Structure and the Phase Transitions of BaTiO<sub>3</sub>*, *Ferroelectrics* **206**, 407 (1998).

- [15] J.-H. Ko, T. H. Kim, K. Roleder, D. Rytz, and S. Kojima, *Precursor Dynamics in the Ferroelectric Phase Transition of Barium Titanate Single Crystals Studied by Brillouin Light Scattering*, Phys. Rev. B **84**, 094123 (2011).
- [16] A. M. Pugachev, V. I. Kovalevskii, N. V. Surovtsev, S. Kojima, S. A. Prosandeev, I. P. Raevski, and S. I. Raevskaya, *Broken Local Symmetry in Paraelectric BaTiO<sub>3</sub> Proved by Second Harmonic Generation*, Phys. Rev. Lett. **108**, 247601 (2012).
- [17] E. K. H. Salje, X. Ding, and O. Aktas, *Domain Glass*, Physica Status Solidi (b) **251**, 2061 (2014).
- [18] S. Hashemizadeh, A. Biancoli, and D. Damjanovic, *Symmetry Breaking in Hexagonal and Cubic Polymorphs of BaTiO<sub>3</sub>*, Journal of Applied Physics **119**, 094105 (2016).
- [19] O. Aktas, S. Crossley, M. A. Carpenter, and E. K. H. Salje, *Polar Correlations and Defect-Induced Ferroelectricity in Cryogenic KTaO<sub>3</sub>* Phys. Rev. B **90**, 165309 (2014).
- [20] E. K. H. Salje, M. A. Carpenter, G. F. Nataf, G. Picht, K. Webber, J. Weerasinghe, S. Lisenkov, and L. Bellaiche, *Elastic Excitations in BaTiO<sub>3</sub> Single Crystals and Ceramics: Mobile Domain Boundaries and Polar Nanoregions Observed by Resonant Ultrasonic Spectroscopy*, Phys. Rev. B **87**, 014106 (2013).
- [21] M. Eremenko, V. Krayzman, A. Bosak, H. Y. Playford, K. W. Chapman, J. C. Woicik, B. Ravel, and I. Levin, *Local Atomic Order and Hierarchical Polar Nanoregions in a Classical Relaxor Ferroelectric*, Nature Communications **10**, 1 (2019).
- [22] J. Harada, J. D. Axe, and G. Shirane, *Neutron-Scattering Study of Soft Modes in Cubic BaTiO<sub>3</sub>*, Phys. Rev. B **4**, 155 (1971).
- [23] I. Tomeno, J. A. Fernandez-Baca, S. Chi, K. Oka, and Y. Tsunoda, *Coexistence of Soft Modes and Dynamic Ti Disorder in Cubic BaTiO<sub>3</sub> Studied by Inelastic Neutron Scattering*, J. Phys. Soc. Jpn. **89**, 054601 (2020).
- [24] A. Belsky, M. Hellenbrandt, V. L. Karen, and P. Luksch, *New Developments in the Inorganic Crystal Structure Database (ICSD): Accessibility in Support of Materials Research and Design*, Acta Cryst B **58**, 364 (2002).
- [25] A. Jain, S. P. Ong, G. Hautier, W. Chen, W. D. Richards, S. Dacek, S. Cholia, D. Gunter, D. Skinner, G. Ceder, and K. A. Persson, *Commentary: The Materials Project: A Materials Genome Approach to Accelerating Materials Innovation*, APL Materials **1**, 011002 (2013).
- [26] S. Kirklin, J. E. Saal, B. Meredig, A. Thompson, J. W. Doak, M. Aykol, S. Rühl, and C. Wolverton, *The Open Quantum Materials Database (OQMD): Assessing the Accuracy of DFT Formation Energies*, Npj Computational Materials **1**, 15010 (2015).
- [27] S. Curtarolo, W. Setyawan, G. L. W. Hart, M. Jahnatek, R. V. Chepulskii, R. H. Taylor, S. Wang, J. Xue, K. Yang, O. Levy, M. J. Mehl, H. T. Stokes, D. O. Demchenko, and D. Morgan, *AFLOW: An Automatic Framework for High-Throughput Materials Discovery*, Computational Materials Science **58**, 218 (2012).
- [28] O. I. Malyi and A. Zunger, *False Metals, Real Insulators, and Degenerate Gapped Metals*, Applied Physics Reviews **7**, 041310 (2020).
- [29] C. M. I. Okoye, *Theoretical Study of the Electronic Structure, Chemical Bonding and Optical Properties of KNbO<sub>3</sub> in the Paraelectric Cubic Phase*, J. Phys.: Condens. Matter **15**, 5945 (2003).
- [30] S. Saha, T. P. Sinha, and A. Mookerjee, *Electronic Structure, Chemical Bonding, and Optical Properties of Paraelectric BaTiO<sub>3</sub>*, Phys. Rev. B **62**, 8828 (2000).
- [31] S. Cabuk, H. Akkus, and A. M. Mamedov, *Electronic and Optical Properties of KTaO<sub>3</sub>: Ab Initio Calculation*, Physica B: Condensed Matter **394**, 81 (2007).
- [32] A. Bencan, E. Oveisi, S. Hashemizadeh, V. K. Veerapandiyan, T. Hoshina, T. Rojac, M. Deluca, G. Drazic, and D. Damjanovic, *Atomic Scale Symmetry and Polar Nanoclusters in the Paraelectric Phase of Ferroelectric Materials*, ArXiv:2010.10860 (2020).
- [33] A. Zunger, *Electronic Structure of 3d Transition-Atom Impurities in Semiconductors*, in *Solid State Physics*, edited by H. Ehrenreich and D. Turnbull, Vol. 39 (Academic Press, 1986), pp. 275–464.
- [34] A. F. Wells, *Structural Inorganic Chemistry* (OUP Oxford, 2012).
- [35] A. Mercy, J. Bieder, J. Íñiguez, and P. Ghosez, *Structurally Triggered Metal-Insulator Transition in Rare-Earth Nickelates*, Nature Communications **8**, 1677 (2017).

- [36] Q. Zhang, T. Cagin, and W. A. Goddard, *The Ferroelectric and Cubic Phases in BaTiO<sub>3</sub> Ferroelectrics Are Also Antiferroelectric*, PNAS **103**, 14695 (2006).
- [37] Z. Wang, X.-G. Zhao, R. Koch, S. J. L. Billinge, and A. Zunger, *Understanding Electronic Peculiarities in Tetragonal FeSe as Local Structural Symmetry Breaking*, Phys. Rev. B **102**, 235121 (2020).
- [38] G. Trimarchi, Z. Wang, and A. Zunger, *Polymorphous Band Structure Model of Gapping in the Antiferromagnetic and Paramagnetic Phases of the Mott Insulators MnO, FeO, CoO, and NiO*, Phys. Rev. B **97**, 035107 (2018).
- [39] X.-G. Zhao, G. M. Dalpian, Z. Wang, and A. Zunger, *Polymorphous Nature of Cubic Halide Perovskites*, Phys. Rev. B **101**, 155137 (2020).
- [40] X. Moya, E. Stern-Taulats, S. Crossley, D. González-Alonso, S. Kar-Narayan, A. Planes, L. Mañosa, and N. D. Mathur, *Giant Electrocaloric Strength in Single-Crystal BaTiO<sub>3</sub>*, Advanced Materials **25**, 1360 (2013).
- [41] G. Burns and F. H. Dacol, *Polarization in the Cubic Phase of BaTiO<sub>3</sub>*, Solid State Communications **42**, 9 (1982).
- [42] V. M. Goldschmidt, *Die Gesetze der Krystallochemie*, Naturwissenschaften **14**, 477 (1926).
- [43] M. Paściak, T. R. Welberry, J. Kulda, S. Leoni, and J. Hlinka, *Dynamic Displacement Disorder of Cubic BaTiO<sub>3</sub>*, Phys. Rev. Lett. **120**, 167601 (2018).
- [44] A. M. Quittet and M. Lambert, *Temperature Dependence of the Raman Cross Section and Light Absorption in Cubic BaTiO<sub>3</sub>*, Solid State Communications **12**, 1053 (1973).
- [45] A. Safari and E. K. Akdogan, *Piezoelectric and Acoustic Materials for Transducer Applications* (Springer, 2008).